

Structural Studies of the Human PBAF Chromatin-Remodeling Complex

Andres E Leschziner,¹ Bryan Lemon,^{2,3}

Robert Tjian,² and Eva Nogales^{1,2,*}

¹Lawrence Berkeley National Laboratory
Berkeley, California 94720

²Department of Molecular and Cell Biology
and Howard Hughes Medical Institute
University of California, Berkeley
Berkeley, California 94720

Summary

ATP-dependent chromatin remodeling is one of the central processes responsible for imparting fluidity to chromatin and thus regulating DNA transactions. Although knowledge on this process is accumulating rapidly, the basic mechanism (or mechanisms) by which the remodeling complexes alter the structure of a nucleosome is not yet understood. Structural information on these macromolecular machines should aid in interpreting the biochemical and genetic data; to this end, we have determined the structure of the human PBAF ATP-dependent chromatin-remodeling complex preserved in negative stain by electron microscopy and have mapped the nucleosome binding site using two-dimensional (2D) image analysis. PBAF has an overall C-shaped architecture—with a larger density to which two smaller knobs are attached—surrounding a central cavity; one of these knobs appears to be flexible and occupies different positions in each of the structures determined. The 2D analysis of PBAF:nucleosome complexes indicates that the nucleosome binds in the central cavity.

Introduction

Cells have developed a variety of mechanisms to deal with the tight packaging of their DNA into chromatin, turning the latter into a highly dynamic entity that can be modulated to affect replication, recombination, DNA repair, and transcription. Chromatin remodeling is a broad term used to refer to a variety of processes responsible for the modulation of chromatin, including modifications of the histone and nonhistone protein contents of chromatin, DNA methylation, covalent modification of histones, and conformational changes of the nucleosomes. This last type of modification is catalyzed by a large family of ATP-dependent chromatin-remodeling complexes. These have been identified in organisms ranging from yeast to humans and can be divided into three subfamilies characterized by the type of catalytic ATPase they contain: SNF2; ISWI, or CHD1 (reviewed in Becker and Horz, 2002; Lusser and Kadonaga, 2003; Narlikar et al., 2002). The SNF2-like containing SWI/SNF complexes include yeast SWI/SNF and RSC as well as their human orthologs, BAF and PBAF, respectively (Wang et al., 1996a; Xue et al., 2000). These are all large (>1 MDa), multisubunit (>10) complexes that use ATP hydrolysis to affect the confor-

mation of nucleosomes leading to a variety of outcomes that include histone octamer sliding or transfer, exposure of nucleosomal DNA, generation of dinucleosome species, and even removal of H2A/H2B histone dimers from the octamer (see Becker and Horz, 2002; Flaus and Owen-Hughes, 2001; Narlikar et al., 2002 and references therein). Three mechanisms have been proposed to account for these observations: bulge diffusion, twist defect propagation (see Flaus and Owen-Hughes, 2003 for a detailed description), and, more recently, wave propagation (a combination of the other two [Saha et al., 2002]). However, the actual mechanism of remodeling, or even whether more than one distinct mechanism is at play, is not yet known.

The mammalian PBAF complex (originally known as SWI/SNF-B) was initially characterized when antibodies raised against the mammalian SNF2 homolog BRG1 were used to purify large complexes from several cell lines and was shown to increase the accessibility of nucleosomal DNA to a transcription factor (Wang et al., 1996a, 1996b). More recently, PBAF and the highly related BAF complex were separated using conventional chromatographic approaches, and the two complexes were shown to differ by the presence of a pair of discriminating subunits (BAF180 and BAF200 in PBAF and BAF250 in BAF) (Lemon et al., 2001). This difference was sufficient to impart the complexes with specificity in a particular transcriptional setting: PBAF, but not BAF, was able to activate vitamin D receptor-dependent transcription on a chromatinized template (Lemon et al., 2001). Several subunits in the SWI/SNF complexes have been shown to be involved in recruitment to and association with chromatin (reviewed in Martens and Winston, 2003 and Becker and Horz, 2002), but we are far from establishing a complete picture of the roles played by the multiple subunits present in these complexes.

A full understanding of the mechanism by which these complex machines are able to remodel chromatin with the observed specificity will require structural information that can complement the growing body of biochemical and genetic data. Because of the difficulty in obtaining large quantities of these complexes, electron microscopy is the structural technique of choice.

Here, we have undertaken the three-dimensional (3D) reconstruction of the human PBAF complex preserved in negative stain as a first step to more detailed structural studies. The complex has an overall C-shaped structure with two knobs protruding from the ends of a larger density, all surrounding a central cavity. One of the knobs appears to be flexible and occupies different positions in each reconstruction determined. We have also used 2D image analysis of PBAF:nucleosome complexes and map the general location of the nucleosome binding site to the central cavity in PBAF.

Results

Random Conical Tilt Reconstruction of PBAF

The human PBAF complex used in this work was purified from its native source (Lemon et al., 2001) and was

*Correspondence: enogales@lbl.gov

³Present Address: Amgen, Inc., South San Francisco, California 94080.

therefore very limiting. Consequently, we decided to undertake the initial 3D reconstruction using material preserved in negative stain where a smaller amount would be required.

Pairs of micrographs of human PBAF preserved in uranyl acetate over a continuous carbon support were collected at 0° and 45° under low-dose conditions. After digitizing the micrographs and extracting approximately 9,500 particles, these were manually edited down to a final set of 5,738 pairs of particles that were used for analysis (see [Experimental Procedures](#) for details).

Initially, we obtained a 3D reconstruction using the angular reconstitution method ([van Heel, 1987](#)) as implemented in the software package IMAGIC ([van Heel et al., 1996](#)) using the 0° tilt data (data not shown). However, we were troubled by the fact that certain reprojections of the structure were not represented in the data at all, particularly those that would have corresponded to the largest (and rather flat) surface of the putative model lying on the carbon support. Although this is not in and of itself an indication that the structure was incorrect, it did suggest that some independent confirmation would be warranted. We were concerned about the possibility of having biochemical and/or conformational heterogeneity in the sample. This would easily lead to an incorrect answer when using angular reconstitution given that we had no prior structural knowledge about the complex to ensure that the class averages selected to be used in angular reconstitution represented different views of a unique object rather than views of different (albeit related) objects.

The best approach to deal with these questions was to determine the structure using the random conical tilt method ([Radermacher et al., 1987](#)) where 3D volumes are obtained for individual classes of particles each representing a characteristic view and where heterogeneities might be identified at the level of the reconstructed class volumes. We subjected the 0° tilt images to alignment and classification (see [Experimental Procedures](#) for details) using, independently, both the IMAGIC and SPIDER ([Frank et al., 1996](#)) software packages. Under the parameters tested, the former appeared to be capable of detecting a greater degree of variability in the data in that more characteristic views were seen in the class averages. We proceeded to obtain 3D reconstructions of all the classes using both the IMAGIC and SPIDER classifications but generating all the volumes using SPIDER. The class membership tables and in-plane rotations obtained in the IMAGIC 2D analysis of the data were converted to SPIDER format. While the most common views resulted in very similar volumes regardless of which software had been used for classification (not shown), only the IMAGIC set allowed us to generate volumes for some of the less common ones. Class volumes were merged whenever appropriate (see [Experimental Procedures](#)). Merging of volumes typically resulted in a reduction of satellite noise, better definition in the major features of the complex, and increased resolution relative to the individual class volumes. We were able to merge up to four volumes in two cases with one of these merged volumes

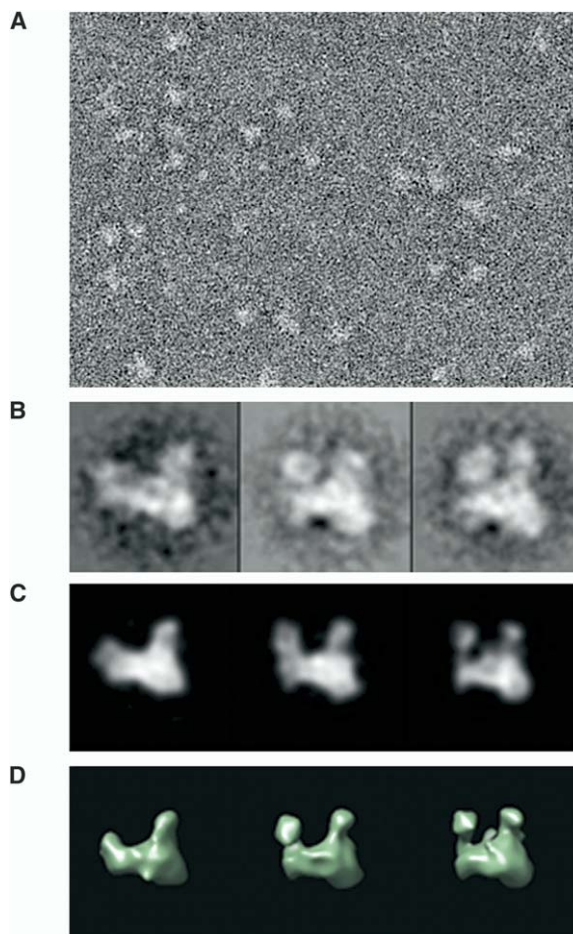


Figure 1. Three-Dimensional Reconstruction of PBAF by the Random Conical Tilt Method

(A) Section of a representative 0° tilt micrograph.
 (B) Representative class averages corresponding to the three reconstructed volumes. Volumes, from 1 to 3, are the result of merging groups of 2, 4, and 2 individual class volumes, respectively; a representative class average from each group is shown here.
 (C) Reprojections of the PBAF volumes in the direction of the class averages.
 (D) Surface rendering of the three reconstructed PBAF volumes (filtered to 50 Å) viewed along the direction of the projections in (C). The volumes (from 1 to 3) are the result of backprojecting 330, 442, and 244 tilted particles. (The total number of particles in the group corresponding to volume 2 was 589, but only the best 75% of particles were used for backprojection—see [Results](#) section for details.)

comprising close to 600 particles (see [Figure 1](#)). However, despite all of our attempts, we were unable to find two volumes whose spatial relationship included a tilt (theta) angle larger than a few degrees. We believe this is the combination of a true preferred orientation of PBAF on the grid and a general flattening of the complex in the stain (see below). Consequently, all of our reconstructions suffer from a significant missing cone.

Five merged volumes were generated ([Figure 1D](#) and [Supplemental Figure S1](#) available with this article online); these volumes account for approximately 36% of the particles in the dataset and are the result of merging

from 2 to 4 individual class volumes such that 15 of the 50 calculated class volumes are part of the volumes presented here. Other volumes were either of poor quality or corresponded to poor class averages. A possible explanation for this is the fact that a relatively small number of classes was used in the last cycle of alignment and classification (50 versus about 350 for other cycles—see [Experimental Procedures](#)) to ensure that enough particles would be present in the volumes; some of the poorer classes may therefore represent a mixture of particles. [Figure 1](#) also shows a section from a representative micrograph (A), a representative class average for each merged volume (B), and reprojections of the volumes in the direction of the class averages (C). Due to the presence in our sample of multiple conformations of PBAF as well as the preferred orientation they adopt on the carbon support (which results in a significant number of views of the complex being absent from our data), we did not carry out a projection-matching refinement of our reconstructions. The volumes presented here were subjected to five cycles of refinement—by crosscorrelation—of the translational parameters of the tilted particles (see [Experimental Procedures](#)). Excluding the 25% of particles with the lowest crosscorrelation coefficient before backprojection only improved the appearance and resolution of volume 2 ([Figures 1 and 2](#)); the renditions of volume 2 shown here are the result of backprojecting 442 of the 589 particles available. All other volumes were generated using the total number of available particles. The resolution of the volumes presented here, as determined by Fourier Shell Correlation ([Saxton and Baumeister, 1982](#); [van Heel and Stoffer-Meilicke, 1985](#)) using the 0.5 criterion, ranged from 43 Å to 50 Å. Consequently, we chose to filter them all to a resolution of 50 Å when rendering the volumes to simplify their comparison.

The exact molecular weight of PBAF is not known. Although the complex has been reported to migrate with an apparent mass of ~2 MDa in gel filtration chromatography ([Kwon et al., 1994](#); [Lemon et al., 2001](#); [Wang et al., 1996a](#)), this estimate may suffer from the fact that molecular weight markers above 600 kDa are not readily available. In fact, the molecular weight of the yeast SWI/SNF complex, determined by a combination of scanning transmission electron microscopy and radiolabeling and stoichiometric analysis ([Smith et al., 2003](#)), was found to be 1.14 MDa (with excellent agreement between the two measurements) instead of the ~2 MDa previously estimated from gel filtration chromatography ([Cote et al., 1994](#)). An estimate of the molecular weight of PBAF—obtained simply by addition of the calculated molecular weights of its subunits and assuming each is present as a single copy in the complex—gives a figure of ~1.15 MDa. This is clearly a lower end estimate as no stoichiometric analysis has been done for PBAF. Simply taking into account the possibility that BAF155 and/or BAF170 might be present as dimers (as shown to be the case for their yeast ortholog Swi3p in the ySWI/SNF complex—[Smith et al., 2003](#)) would bring the molecular weight of the complex to at least 1.4 MDa. The volumes presented here were rendered with a threshold that resulted in reasonable connectivity between the different features while elimi-

nating satellite noise. This threshold corresponds to a molecular weight of 1.35 MDa assuming a protein density of 1.35 g/cm³. This molecular weight should only be taken as a crude approximation since volumes were obtained from negatively stained samples.

Different views of volumes 1–3 are shown in [Figure 2](#). The complex consists of a lopsided base (which we will refer to as the platform) from which two knobs protrude ([Figures 2A and 2B](#)). The platform has a rather large and bulky end and it tapers rather sharply toward the other, thin, end. The two knobs protrude from what we will refer to as the top of the platform and point in the same general direction. The overall dimensions of the complex are approximately 250 Å by 190 Å by 140 Å.

A few major observations can be made from [Figure 2](#). First, these volumes are different yet clearly related, confirming our suspicions about sample heterogeneity and providing a potential explanation for some of the inconsistencies observed with the model obtained using angular reconstitution. In fact, although the volumes presented here and that obtained with angular reconstitution share certain common features (not shown), other differences are significant and clearly show that the initial structure was incorrect. Second, a feature that was quickly evident in all the reconstructed volumes was a considerable flattening of the surface lying on the carbon support ([Figures 2C and 2D](#)). Because of the preferred orientation of PBAF on the grid, we cannot estimate the extent of the flattening as we are unable to compare volumes that are related by any significant tilt angle (i.e., a rotation about an axis lying on the sample plane). Third, another noticeable feature of the volumes is the apparent flexibility of the knob attached to the thinner end of the base (K_1 in [Figure 2A](#)) and the fact that it is usually connected to the base by density that is thinner than that connecting the more stationary knob (K_2). Conformations range from the open one seen in volume 1 ([Figure 2](#)) to a much more closed one seen in volume 3 ([Figure 2](#)). The large scale of this conformational variability is more clearly depicted in [Figure 3](#). Difference maps were calculated between volumes 1 and 3, the two extreme conformations, by subtracting each volume from the other (see [Experimental Procedures](#)): the blue density ([Figure 3](#)) shows the positive peak after subtracting volume 3 from volume 1 (indicating the position of K_1 in volume 1), and the red density corresponds to the positive peak after subtracting volume 1 from volume 3 (indicating the position of K_1 in volume 3). The common core for the two volumes (composed of the platform, P, and the static knob, K_2 , and shown in green mesh) was obtained by adding the normalized volumes together and displaying the resulting volume with a threshold that was twice that used for the individual ones. The distance between the blue and red peaks shown in the map is approximately 90 Å. The K_1 knob appears to be directly attached to the platform in volume 1 (i.e., without the thin P- K_1 connection seen in volumes 2 and 3), but we cannot establish at this point whether this indicates a swinging of the globular end of K_1 about a more static connector (as might be suggested by the short rod-like feature seen between the blue and red densities in the common core in [Figure 3](#)) or a collapse or partial breakdown of K_1 .

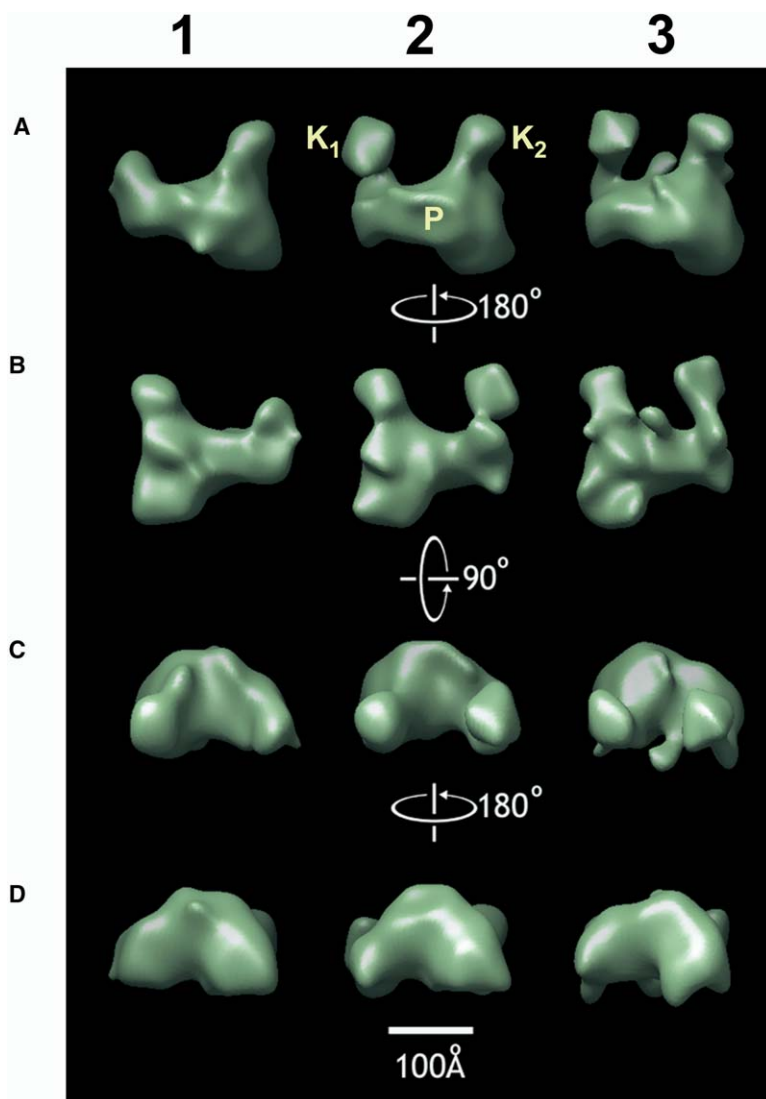


Figure 2. Surface Rendition of Three Different PBAF Volumes

The three volumes depicted in Figure 1D are shown here from four different viewpoints. Row A shows the volumes in the same orientation as in Figure 1D, as seen along the beam axis. The volumes were rotated first by 180° about a vertical axis parallel to the page (B), then by 90° about a horizontal axis parallel to the page (C) bringing the knobs at the top of the volumes toward the front of the page, and finally by 180° about a vertical axis parallel to the page (D). The views shown here will be referred to throughout the text as front (A), back (B), top (C), and bottom (D). The flattening of the complex is most clearly seen in (C) and (D) where volumes are seen along an axis parallel to the grid. The two knobs (K_1 and K_2) and the platform (P) are labeled for volume 2, row A. A 100 \AA scale bar is shown at the bottom of the figure.

In addition to the three volumes presented in Figures 1 and 2, we generated two additional volumes (Supplemental Figure S1) representing less common views of the complex. Although these volumes have the same overall appearance as the other three, the platform is narrower along the horizontal axis (as shown in Figures 1 and 2), and the apparently flexible knob K_1 comes off the base closer to K_2 , approximately $1/3$ in from the thinner end of the platform. In both cases the knobs are less well defined and their shapes differ to varying degrees from those seen in volumes 1–3. It is a distinct possibility that these volumes are slightly tilted views of the more common PBAF orientation represented by volumes 1–3 but that due to the staining-induced flattening of the complex we were unable to merge them with any of the other volumes.

Two-Dimensional Analysis of PBAF: Nucleosome Complexes

After obtaining the initial 3D models of PBAF, we were interested in addressing the question of where the

binding site for the nucleosome was located in the complex. To this end, we prepared a sample consisting of PBAF and recombinant nucleosomes. The nucleosomes were assembled following standard protocols (Luger et al., 1999) using bacterially expressed *X. laevis* histones and a 209 bp fragment of the sea urchin 5S rDNA (see Experimental Procedures for details). The components were mixed under conditions close to those used in remodeling reactions (Lemon et al., 2001), and grids were prepared following the same protocol used for the PBAF sample. Tilt pairs were collected as before. We used the untilted data to carry out a number of cycles of multivariate statistical analysis (MSA) and classification followed by multireference alignment (MRA) using class averages as references. We obtained class averages with clear extra density that could correspond to the added nucleosome (see Supplemental Figure S2) but were concerned that reference bias was being introduced as we enriched the pool of class averages used as references in each iteration with images containing a putative nucleosome. In

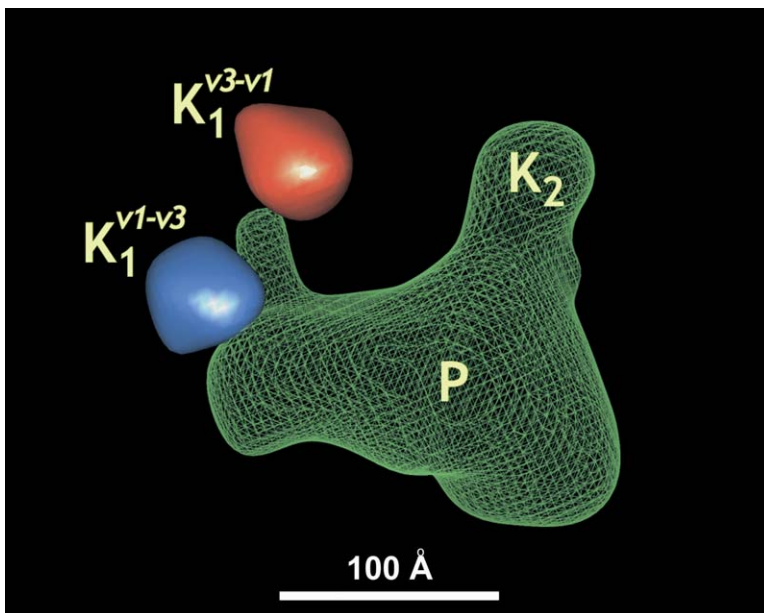


Figure 3. Difference Map Showing the Change in Position of Knob K_1 between Volumes 1 and 3

Difference maps were calculated between the volumes 1 and 3 shown in Figures 1 and 2. Positive density peaks (corresponding to the K_1) are shown for the two difference maps: red for volume 1 subtracted from volume 3 ($v_3 - v_1$) and blue for volume 3 subtracted from volume 1 ($v_1 - v_3$). The part of the structure common to both volumes is shown as a green mesh (see Experimental Procedures for details). The knob (K_2) and platform (P) of the common core are indicated. A 100 Å scale bar is shown at the bottom of the figure.

fact, when a cycle of MRA and classification was performed using either PBAF or PBAF + PBAF:nucleosome references, a significantly larger proportion of class averages containing a putative nucleosome was observed in the latter case. We decided instead to use reprojections of the PBAF volumes—which should be of better quality than class averages—and perform a single cycle of alignment and classification (see Experimental Procedures for details). Inspection of the class averages after this cycle confirmed our initial observation that occupancy by the nucleosome was very low (a few percent), but we were still able to identify a few class averages where a density not observed during the 2D analysis of the PBAF alone data was clearly present (Figures 4A–4C). The extra density we observed in the 2D class averages was exclusively found between the two knobs (Figure 4C) and is commensurate with the dimensions expected from a nucleosome (Figure 4D). Because of the low occupancy by the nucleosome (and because of the preferred orientation as well as the expected flattening), we did not attempt a 3D reconstruction of the PBAF:nucleosome complexes.

Discussion

We have presented here a 3D reconstruction of the human PBAF complex preserved in negative stain obtained by the random conical tilt method as well as 2D mapping of the nucleosome binding site in the complex.

Two other 3D reconstructions of ATP-dependent chromatin-remodeling complexes have been published to date: the yeast RSC complex (Asturias et al., 2002) and the yeast SWI/SNF complex (Smith et al., 2003), the former being the ortholog of human PBAF (Xue et al., 2000). Although all complexes were imaged in negative stain, the reconstructions were obtained using different approaches: ySWI/SNF was solved using an angular reconstitution approach to obtain the initial model

while RSC was reconstructed using the random conical tilt method used here for PBAF. We find that our structure is reminiscent, in its overall architecture, of that of RSC while being completely different from ySWI/SNF. Both RSC and PBAF are C-shaped structures surrounding a central cavity. In the case of RSC, four centers of mass, relatively similar to each other in size, are separated by clear constrictions in the density (see Figure 2 in Asturias et al., 2002). In PBAF, on the other hand, the platform could be considered as two centers of density of unequal size with a thicker connection between them, the remaining two centers of density corresponding to the knobs K_1 and K_2 . Interestingly, Asturias et al. observed that one of the terminal centers of density in RSC was either absent from or appeared collapsed in some of their reconstructions (Asturias et al., 2002). We have similarly observed that K_1 in PBAF appears in different positions relative to the rest of the complex in different reconstructions.

It is difficult to explain the dramatic structural differences seen between RSC or PBAF and ySWI/SNF. Although ySWI/SNF shows a surface depression that has been proposed as the nucleosome binding site (Smith et al., 2003), it shows no evidence of a cavity analogous to the one present in RSC and PBAF or of any other common features. This is not likely a result of using too low a threshold when rendering the ySWI/SNF volume as this was chosen to account for the molecular weight determined experimentally (Smith et al., 2003). On the other hand, one of the ySWI/SNF class averages presented by Smith et al. is strikingly similar to the most common view of PBAF: it shows what appears to be a stretch of continuous density that is thicker at one end (reminiscent of the platform of PBAF) to which two somewhat spherical densities seem to be attached by thin connections (compare class averages 2 and 3 in Figure 1 with the third class average in Figure 4B in Smith et al., 2003). However, the 3D reconstructions of

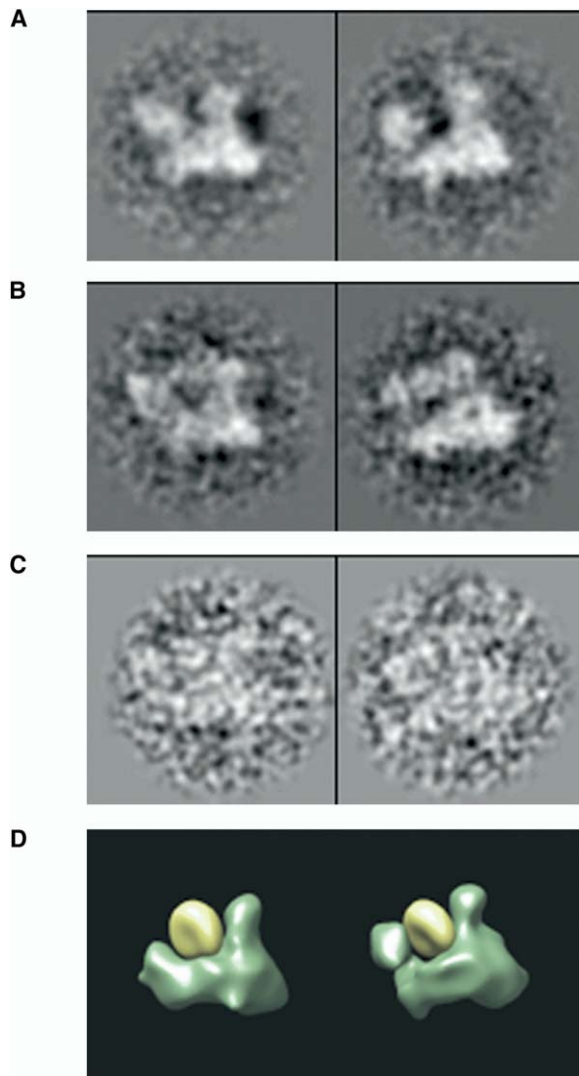


Figure 4. Two-Dimensional Analysis of PBAF:Nucleosome Complexes

- (A) Class averages of PBAF alone.
 (B) Comparable class averages containing additional density.
 (C) Single particle images belonging to the class averages shown in (B).
 (D) Models of PBAF with an added nucleosome. Volumes 1 and 2 from Figure 2 are depicted with a nucleosome placed in the area identified as the binding pocket in (B); the nucleosome was placed manually and is included only as an indication of relative scale.

ySWI/SNF and PBAF that should be giving rise to this characteristic view share no similarity whatsoever.

Structural variability is certainly to be expected among these complexes; they come from different organisms, have different compositions, and show genetic and biochemical differences. Yet, given the degree of conservation among them (Becker and Horz, 2002 and references therein) and the similarity among some of the class averages discussed above, a certain resemblance in their overall architecture seems a reasonable expectation as well. The fact that this expectation is borne out by the structures of PBAF and RSC would

suggest that ySWI/SNF should also share some of the same general features. We believe the absence of any similarity between PBAF/RSC and ySWI/SNF is likely to have arisen as a result of the different approaches used to build a 3D model from the 2D data. Both Asturias et al. and our group have observed a variety of conformations in the complexes in our samples; these differences can only be easily detected using the random conical tilt method for 3D reconstruction (in particular when dealing with asymmetric particles of unknown structure). The advantage of this method is that 3D reconstructions are generated for each separate characteristic view and the angular relationships among the tilted particles used in the reconstructions are determined by the tilt geometry and the usually robust 2D analysis of the data. No assumptions are made regarding a common origin for the different reconstructed volumes and any relationships among them are assessed only after they have been generated. On the other hand, the angular reconstitution method works on the assumption that the input data represent a series of characteristic views of a unique structure; if this is not true, its successful application would require some prior knowledge of the structure in order to avoid selecting for the initial reconstruction views that correspond to different 3D objects. We experienced this difficulty in our initial reconstruction of PBAF using angular reconstitution; the views shown as 1 and 2/3 in Figure 1—which we now know represent the same view of two different conformations of PBAF—were taken as orthogonal views of the complex (about a vertical axis as they are shown), leading to an incorrect structure. It is noteworthy that our initial incorrect structure still yielded reprojections that matched the input data (data not shown); therefore, this fact alone was not a good indication of the correctness of the structure. In this respect, a match between a reprojection along the beam axis of a volume reconstructed by the random conical tilt method and its corresponding class average is a much better indication of the quality of the reconstruction; the 0° tilt particles used for the 2D analysis do not participate in the generation of the class volumes which consist entirely of tilted particles.

In addition to the overall architectural similarity between RSC and PBAF, our nucleosome mapping data—positioning the nucleosome in the central cavity of the complex—are in agreement with a model proposed for RSC (Asturias et al., 2002). However, our data are inconsistent with the nucleosome binding site proposed for ySWI/SNF. Given that the similarities in the class averages of PBAF and ySWI/SNF are very likely to represent true similarities between the complexes, the proposed binding site for the nucleosome in ySWI/SNF predicts that class averages should show the density corresponding to the nucleosome on the side of the platform of PBAF opposite to that where we have actually observed it (Figure 4).

The use of random conical tilt as a strategy for 3D reconstruction has allowed us to identify a number of concomitant conformations in our human PBAF samples. It is not clear at this point what the meaning is of the flexibility observed in one of the PBAF knobs. It is tempting to speculate that this flexibility might be biologically relevant, especially in light of where the

nucleosome appears to bind. Movement of one of the knobs involved in nucleosome binding could be part of the remodeling cycle, perhaps by allowing alternative binding modes. However, due to the fact that these samples were preserved in negative stain and subjected to flattening, it is not possible at this time to discard the possibility of artifactual movement. Obtaining a 3D reconstruction of PBAF in vitrified ice will allow us to address this question. In addition, obtaining higher occupancy of the nucleosome in PBAF for 3D reconstruction and mapping of subunits should be immediate priorities to tie the wealth of genetic and biochemical data to what is only the very early stages of a structural understanding of ATP-dependent chromatin remodeling.

Experimental Procedures

Preparation of PBAF and Nucleosomes

The human PBAF complex was purified as published (Lemon et al., 2001). Aliquots were thawed right before application to the grid and diluted to a final concentration of PBAF of approximately 20 $\mu\text{g}/\text{ml}$. The final conditions in the sample were 20 mM HEPES (pH 7.9); 150 mM KCl; 5% glycerol; 2 mM MgCl_2 ; 0.2 mM EDTA; 0.01% NP-40; and 14 $\mu\text{g}/\text{ml}$ lysozyme as carrier. Typically, 5 μl of sample were applied to carbon-coated 400-mesh copper grids (Ted Pella, Inc, Redding, California) that were glow-discharged for 20–25 s immediately before use, were allowed to adsorb for 2 min, and the grids were twice blotted and rinsed with 5 μl of 20 mM HEPES (pH 7.9); 100 mM KCl; 5% trehalose; 2 mM MgCl_2 ; 0.2 mM EDTA; and 0.01% NP-40. Grids were finally rinsed in ddH_2O , blotted, and stained with 3% uranyl acetate for 1 min.

Nucleosomes were prepared following standard protocols (Luger et al., 1999). Briefly, histones H2A, H2B, H3, and H4 from *X. laevis* were overexpressed separately in *E. coli* BL21(DE3)[pLysS] (Promega) and the inclusion bodies were denatured in urea and run over a Superdex 75 gel filtration column (Amersham Biosciences). The peak fractions were pooled, dialyzed, and lyophilized and then run under denaturing conditions over a Poros HS column (Amersham Biosciences). Peak fractions were pooled, dialyzed, and lyophilized again. Yields ranged from 6.5 mg to 45 mg of histone for each initial 1.5 liter of bacterial culture. The four histones were then resuspended in denaturing buffer and mixed in equimolar amounts with a slight excess of H2A/H2B (Luger et al., 1999). The samples were then refolded by dialysis and histone octamers were resolved on a Superdex 200 gel filtration column (Amersham Biosciences). Nucleosomal DNA was generated from plasmid pIC-20B5S-G5E4 (Ikeda et al., 1999) containing 12 tandemly repeated copies of the sea urchin 5S rDNA. Two hundred and nine basepair fragments containing the 5S rDNA nucleosome-positioning sequence were excised by restriction digest; the plasmid backbone was removed by precipitating it with polyethylene glycol (Lis, 1980), and the 5S rDNA-containing fragments were purified away from other small products by electrophoresis over a native 8% polyacrylamide gel in TBE buffer in a Model 491 prep cell (BioRad, Richmond, California). A final 3.4 mg of fragment were obtained from an initial 37 mg of plasmid. The DNA fragment and histone octamers were mixed in at a 1.1:1 molar DNA:octamer ratio in 2 M KCl and the salt concentration was lowered to 0.25 M by gradient dialysis over 18 hr at 4°C (Luger et al., 1999). The dialysate was concentrated to a final 1.4 mg/ml and incubated at 37°C for 1 hr to reposition the histone octamers. The sample was electrophoresed over a 5% native polyacrylamide gel in 0.2 \times TBE buffer to separate nucleosomes from free DNA. The peak containing nucleosomes was concentrated to about 4.5 mg/ml, exchanged into 20 mM TrisHCl (pH 7.5); 1 mM EDTA; and 1 mM DTT, and stored at -80°C . Analysis of the purified nucleosomes by agarose gel electrophoresis revealed the presence of two major faster species and one minor slower one.

PBAF and nucleosomes were mixed at different ratios, with nucleosomes always in molar excess and PBAF at a final concentration of 26 $\mu\text{g}/\text{ml}$. Because the components were in different stor-

age buffers and dialysis of small volumes of PBAF had resulted in very poor sample quality, the final sample contained a mixture of 3.5 mM HEPES (pH 7.9); 16.5 mM HEPES (pH 7.6); and 2 mM TrisHCl (pH 7.5). The sample also contained 0.35 mM MgCl_2 ; 5% glycerol; 2 mM EDTA; 0.01% NP-40; 100 mM KCl; 1 mM DTT; and 17.5 $\mu\text{g}/\text{ml}$ lysozyme. After mixing, samples were incubated at 30°C for 15 min and grids were prepared as for PBAF alone (see above).

Microscopy and Digitization of Micrographs

Data were collected on a Tecnai 12 (FEI Company) microscope operated at 120 keV on Kodak SO-163 film under low-dose conditions at a nominal magnification of either 30,000 \times (PBAF alone) or 49,000 \times (PBAF:nucleosome) with underdefocus ranging from 0.5 μm to 1.5 μm . The tilt angle was typically -45° . Micrographs were digitized in a Nikon Super Coolsan 8000 (PBAF alone data) or a LeafScan 45 scanner (PBAF:nucleosome) with scanning resolutions of 12.71 $\mu\text{m}/\text{pixel}$ and 10 $\mu\text{m}/\text{pixel}$, respectively, resulting in resolutions of 4.24 $\text{\AA}/\text{pixel}$ (PBAF) and 2.04 $\text{\AA}/\text{pixel}$ (PBAF:nucleosome) at the level of the sample. The PBAF:nucleosome data were decimated 2-fold to a resolution of 4.08 $\text{\AA}/\text{pixel}$.

PBAF: Two-Dimensional Data Analysis with IMAGIC

Particle coordinates were established interactively using WEB, the graphic interface of SPIDER (Frank et al., 1996). Particles were extracted using a box size of 144 \times 144 pixels and normalized by matching a noise histogram. The initial set of approximately 9,500 particles was culled down to 5,738 particles, removing particles with low contrast as well as those whose tilted counterparts had very low defoci or defoci that were high enough to place the first zero of the CTF at frequencies below 1/30 \AA . The particles were then converted to IMAGIC format using the EM2EM program in IMAGIC (van Heel et al., 1996) and then low-pass and high-pass filtered using Gaussian filters with midpoint frequencies of 1/19 \AA^{-1} and 1/450 \AA^{-1} , respectively (these values were determined empirically by testing their effect on the subsequent alignment and classification). Images were thresholded to reduce extreme negative values, which are most likely due to stain artifacts (particles were visually inspected to determine the threshold value). Particles were centered in the window according to their center of mass and were then subjected to MSA and hierarchical ascendant classification. Classes that contained on average 19 particles/class (corresponding to the largest possible number of classes that did not result in apparently duplicated class averages) were generated and good class averages were selected visually. We sought to select as many different views as possible and only eliminated class averages that appeared featureless, were too large or too small, or had significantly blurred edges. All selected classes were manually edited to remove particles that seemed to have been incorrectly assigned to the class, and those averages that were still of good quality after editing (33 in total) were selected (we later determined that this culling has little effect in the classification results). These class averages (and their mirror images) were normalized and centered and a soft mask was applied to them. The entire dataset was then aligned rotationally and translationally against these references and subjected again to MSA and classification. Three additional cycles of MRA, MSA, and classification were performed. Typically, 34–39 class averages were selected as references for the next MRA. Starting at the second cycle, the MRA references were both centered and rotationally aligned (the latter improved the quality of the subsequent class averages significantly). Classifications were set up to generate classes containing on average 15–20 particles per class except in the last iteration where only 50 classes (with an average of 115 particles/class) were generated in preparation for the reconstruction of class volumes (where a relatively large number of particles per class is required). At this point, SPIDER-format files containing the X- and Y-shifts and in-plane rotations from the last cycle of MRA as well as the class membership information from the last cycle of MSA were created.

PBAF: Three-Dimensional Data Analysis with SPIDER

Sets with untilted and tilted particles with 147 \times 147 pixel boxes were generated in SPIDER. The particles were low-pass and high-pass filtered using Butterworth filters with the same frequency cut-

offs as those used in IMAGIC (see above). The translational and rotational parameters obtained from the 2D analysis in IMAGIC were applied to the untilted particles in order to check the parameters transferred by regenerating the class averages. The in-plane rotation was also combined with the angles from the tilt geometry to generate a set of Euler angles to be used in the reconstructions with the tilted particles. Each particle was centered by crosscorrelating it against its own rotational average; the centering was iterated until the shifts became zero. Volumes were generated for all 50 classes using the class membership information obtained in the 2D analysis in IMAGIC. All calculations of volumes discussed here included five iterations of refinement where the translational parameters of the tilted particles were refined by crosscorrelation between each tilted particle and the corresponding reprojection of the volume in its direction. A 3D search (involving rotation and cross-correlation) was performed for all possible pairwise combinations of volumes. Crosscorrelation coefficients and visual inspection were used to divide the class volumes into groups within which mergers would be attempted as well as to decide which pairs would be merged first. After each merger, a new 3D search was performed between the merged volume and the remaining members of the group. Volumes continued to be merged until the cross-correlation coefficients seemed to drop significantly and/or merging of an additional volume resulted in a drastic loss of (broad) features in the merged volume relative to the previous merged volume. The resolution of a given merged volume was determined by generating half-volumes (using the odd- and even-numbered particles) and calculating the Fourier Shell Correlation (Saxton and Baumeister, 1982; van Heel and Stoffer-Heilicke, 1985) between them. The resolutions reported here correspond to the 0.5 FSC criterion.

PBAF:Nucleosome: Two-Dimensional Analysis with IMAGIC

PBAF:nucleosome particles were selected and windowed out using EMAN's Boxer (Ludtke et al., 1999) and a box size of 100 × 100 pixels. Particles (10,723) were prepared as described above for the PBAF data (except that a slightly stronger low-pass filtration—with a midpoint frequency of 1/20 in the Gaussian filter—was used in this case to improve the lower contrast of this dataset) and were then subjected to MRA IMAGIC using reprojections of the reconstructed PBAF volumes as references (see Results). The PBAF volumes were low-pass filtered to a resolution of 1/50 Å⁻¹ and then threshold-masked (with the masks filtered using the same parameters applied to the volumes). Several projections were generated for each volume ranging from 0° (the direction of the class average) to 25° tilt to cover a range of potential orientations of the particles. Eventually, the 0° and 25° projections of each particle were chosen (they were different enough from each other while still representing common PBAF views) and used for a single cycle of MRA followed by a cycle of MSA and hierarchical ascendant classification. The best classification of the dataset was obtained for classes with an average of 20–35 particles/class. Classes showing densities not seen in the PBAF alone class averages were selected for further inspection. This subset of classes was visualized and the classes whose extra density was reduced after particle editing were discarded. The data shown in Supplemental Figure S2 were obtained using IMAGIC and the same approach taken for the 2D analysis of the PBAF alone data. More specifically, after an initial MSA and hierarchical ascendant classification, four cycles of MRA and MSA/classification were performed and the set of references used for the MRA's was enriched in class averages containing a putative nucleosome in every cycle. The class averages shown in Supplemental Figure S2 are the output of a classification that resulted in an average of 30 particles/class.

Volume Rendering

The volumes presented here were low-pass filtered as described in the previous section. For display, volumes were thresholded to account for a molecular weight of 1.35 MDa assuming a protein density of 1.35 g/cm³. The nucleosome used in Figure 4 is the structure obtained by Luger et al. (1997) (accession number 1AOI). The PDB file was converted to SPIDER format, filtered using the same parameters applied to the volumes, and thresholded to ac-

count for a molecular weight of 210 kDa. Molecular graphics images were produced using the UCSF Chimera package from the Computer Graphics Laboratory, University of California, San Francisco (supported by NIH P41 RR-01081) (Pettersen et al., 2004).

Difference Map

Volume 3 was aligned relative to volume 1 by applying X- and Y-shifts and in-plane rotation obtained from a 2D alignment performed between 0,0,0 projections of the volumes with portions outside the common platform and static knob (P and K₂, respectively, in Figure 2) masked out. The volumes were normalized and subtracted from each other (volume 1 – volume 3 and volume 3 – volume 1) to generate the difference maps. The highest peaks in the difference maps are shown in Figure 4. The common core (P + K₂) was generated by adding the two volumes together and thresholding the resulting volume using a value that was twice that used for the individual volumes. Volumes were rendered using the UCSF Chimera package from the Computer Graphics Laboratory, University of California, San Francisco (supported by NIH P41 RR-01081) (Pettersen et al., 2004).

Supplemental Data

Supplemental Data include two figures and can be found with this article online at <http://www.structure.org/cgi/content/full/13/2/267/DC1/>.

Acknowledgments

We would like to thank Patricia Meurer-Groß for suggestions about the manuscript. A.E.L. was supported by an Agouron Institute fellowship from the Jane Coffin Childs Memorial Fund for Medical Research. B.L. was supported in part by a National Research Service Award. R.T. and E.N. are investigators of the Howard Hughes Medical Institute.

Received: November 5, 2004

Revised: December 16, 2004

Accepted: December 17, 2004

Published: February 8, 2005

References

- Asturias, F.J., Chung, W.H., Kornberg, R.D., and Lorch, Y. (2002). Structural analysis of the RSC chromatin-remodeling complex. *Proc. Natl. Acad. Sci. USA* 99, 13477–13480.
- Becker, P.B., and Horz, W. (2002). ATP-dependent nucleosome remodeling. *Annu. Rev. Biochem.* 71, 247–273.
- Cote, J., Quinn, J., Workman, J.L., and Peterson, C.L. (1994). Stimulation of GAL4 derivative binding to nucleosomal DNA by the yeast SWI/SNF complex. *Science* 265, 53–60.
- Flaus, A., and Owen-Hughes, T. (2001). Mechanisms for ATP-dependent chromatin remodeling. *Curr. Opin. Genet. Dev.* 11, 148–154.
- Flaus, A., and Owen-Hughes, T. (2003). Mechanisms for nucleosome mobilization. *Biopolymers* 68, 563–578.
- Frank, J., Radermacher, M., Penczek, P., Zhu, J., Li, Y., Ladjadj, M., and Leith, A. (1996). SPIDER and WEB: processing and visualization of images in 3D electron microscopy and related fields. *J. Struct. Biol.* 116, 190–199.
- Ikeda, K., Steger, D.J., Eberharter, A., and Workman, J.L. (1999). Activation domain-specific and general transcription stimulation by native histone acetyltransferase complexes. *Mol. Cell. Biol.* 19, 855–863.
- Kwon, H., Imbalzano, A.N., Khavari, P.A., Kingston, R.E., and Green, M.R. (1994). Nucleosome disruption and enhancement of activator binding by a human SW1/SNF complex. *Nature* 370, 477–481.
- Lemon, B., Inouye, C., King, D.S., and Tjian, R. (2001). Selectivity of chromatin-remodelling cofactors for ligand-activated transcription. *Nature* 414, 924–928.

- Lis, J.T. (1980). Fractionation of DNA fragments by polyethylene glycol induced precipitation. *Methods Enzymol.* **65**, 347–353.
- Ludtke, S.J., Baldwin, P.R., and Chiu, W. (1999). EMAN: semiautomated software for high-resolution single-particle reconstructions. *J. Struct. Biol.* **128**, 82–97.
- Luger, K., Mader, A.W., Richmond, R.K., Sargent, D.F., and Richmond, T.J. (1997). Crystal structure of the nucleosome core particle at 2.8 Å resolution. *Nature* **389**, 251–260.
- Luger, K., Rechsteiner, T.J., and Richmond, T.J. (1999). Preparation of nucleosome core particle from recombinant histones. *Methods Enzymol.* **304**, 3–19.
- Lusser, A., and Kadonaga, J.T. (2003). Chromatin remodeling by ATP-dependent molecular machines. *Bioessays* **25**, 1192–1200.
- Martens, J.A., and Winston, F. (2003). Recent advances in understanding chromatin remodeling by Swi/Snf complexes. *Curr. Opin. Genet. Dev.* **13**, 136–142.
- Narlikar, G.J., Fan, H.Y., and Kingston, R.E. (2002). Cooperation between complexes that regulate chromatin structure and transcription. *Cell* **108**, 475–487.
- Pettersen, E.F., Goddard, T.D., Huang, C.C., Couch, G.S., Greenblatt, D.M., Meng, E.C., and Ferrin, T.E. (2004). UCSF Chimera—a visualization system for exploratory research and analysis. *J. Comput. Chem.* **25**, 1605–1612.
- Radermacher, M., Wagenknecht, T., Verschoor, A., and Frank, J. (1987). Three-dimensional reconstruction from a single-exposure, random conical tilt series applied to the 50S ribosomal subunit of *Escherichia coli*. *J. Microsc.* **146**, 113–136.
- Saha, A., Wittmeyer, J., and Cairns, B.R. (2002). Chromatin remodeling by RSC involves ATP-dependent DNA translocation. *Genes Dev.* **16**, 2120–2134.
- Saxton, W.O., and Baumeister, W. (1982). The correlation averaging of a regularly arranged bacterial cell envelope protein. *J. Microsc.* **127**, 127–138.
- Smith, C.L., Horowitz-Scherer, R., Flanagan, J.F., Woodcock, C.L., and Peterson, C.L. (2003). Structural analysis of the yeast SWI/SNF chromatin remodeling complex. *Nat. Struct. Biol.* **10**, 141–145.
- van Heel, M. (1987). Angular reconstitution: a posteriori assignment of projection directions for 3D reconstruction. *Ultramicroscopy* **21**, 111–123.
- van Heel, M., and Stoffler-Meilicke, M. (1985). Characteristic views of *E. coli* and *B. stearothermophilus* 30S ribosomal subunits in the electron microscope. *EMBO J.* **4**, 2389–2395.
- van Heel, M., Harauz, G., Orlova, E.V., Schmidt, R., and Schatz, M. (1996). A new generation of the IMAGIC image processing system. *J. Struct. Biol.* **116**, 17–24.
- Wang, W., Cote, J., Xue, Y., Zhou, S., Khavari, P.A., Biggar, S.R., Muchardt, C., Kalpana, G.V., Goff, S.P., Yaniv, M., et al. (1996a). Purification and biochemical heterogeneity of the mammalian SWI-SNF complex. *EMBO J.* **15**, 5370–5382.
- Wang, W., Xue, Y., Zhou, S., Kuo, A., Cairns, B.R., and Crabtree, G.R. (1996b). Diversity and specialization of mammalian SWI/SNF complexes. *Genes Dev.* **10**, 2117–2130.
- Xue, Y., Canman, J.C., Lee, C.S., Nie, Z., Yang, D., Moreno, G.T., Young, M.K., Salmon, E.D., and Wang, W. (2000). The human SWI/SNF-B chromatin-remodeling complex is related to yeast rsc and localizes at kinetochores of mitotic chromosomes. *Proc. Natl. Acad. Sci. USA* **97**, 13015–13020.